THE JOURNAL OF BIOLOGICAL CHEMISTRY VOL. 289, NO. 46, pp. 31914–31926, November 14, 2014

Diacylglycerol Kinase α Regulates Tubular Recycling Endosome Biogenesis and Major Histocompatibility Complex Class I Recycling*[S]

Received for publication, July 3, 2014, and in revised form, September 12, 2014 Published, JBC Papers in Press, September 23, 2014, DOI 10.1074/jbc.M114.594291

Shuwei Xie, Naava Naslavsky[1], and Steve Caplan[2]

From the Department of Biochemistry and Molecular Biology and the Fred and Pamela Buffett Cancer Center, The University of Nebraska Medical Center, Omaha, Nebraska 68198

Background: Major histocompatibility complex class I (MHC I) trafficking is crucial for antigen presentation.
Results: Diacylglycerol kinase α (DGKα) depletion interferes with tubular recycling endosome (TRE) biogenesis and delays MHC I recycling to the plasma membrane.
Conclusion: DGKα mediates MHC I recycling by interacting with MICAL-L1 and generating phosphatidic acid.
Significance: A novel role for DGKα in generating phosphatidic acid for TRE biogenesis and MHC I recycling.

Major histocompatibility complex class I (MHC I) presents intracellular-derived peptides to cytotoxic T lymphocytes and its subcellular itinerary is important in regulating the immune response. While a number of diacylglycerol kinase isoforms have been implicated in clathrin-dependent internalization, MHC I lacks the typical motifs known to mediate clathrin-dependent endocytosis. Here we show that depletion of diacylglycerol kinase α (DGKα), a kinase devoid of a clathrin-dependent adaptor protein complex 2 binding site, caused a delay in MHC I recycling to the plasma membrane without affecting the rate of MHC I internalization. We demonstrate that DGKα knock-down causes accumulation of intracellular and surface MHC I, resulting from decreased degradation. Furthermore, we provide evidence that DGKα is required for the generation of phosphatidic acid required for tubular recycling endosome (TRE) biogenesis. Moreover, we show that DGKα forms a complex with the TRE hub protein, MICAL-L1. Given that MICAL-L1 and the F-BAR-containing membrane-tubulating protein Syndapin2 associate selectively with phosphatidic acid, we propose a positive feedback loop in which DGKα generates phosphatidic acid to drive its own recruitment to TRE via its interaction with MICAL-L1. Our data support a novel role for the involvement of DGKα in TRE biogenesis and MHC I recycling.

Major histocompatibility complex class I (MHC I)[3] molecules are an essential component of the cellular immune response to a variety of intracellular pathogens and tumors. Expressed on the surface of all cells, MHC I molecules present foreign peptide antigens to cytotoxic T lymphocytes, resulting in an immune response and the killing of the infected or tumor cell (reviewed in Ref. 1). Accordingly, expression of functional peptide-loaded MHC I on the plasma membrane depends upon the rate of MHC I synthesis, assembly and peptide binding, and the rate at which MHC I molecules are internalized from the plasma membrane.

The classic and best-characterized mode by which receptors are internalized from the plasma membrane is through clathrin-coated pits. However, some plasma membrane proteins, including MHC I, are devoid of conventional clathrin-dependent endocytosis signals, and occur along a pathway regulated in part by the small GTP-binding protein ADP-ribosylation factor 6 (Arf6) (2). Although many advances have been made in deciphering the internalization and subsequent trafficking of clathrin-independent cargo, our understanding of these pathways nonetheless lags behind the more extensive knowledge of clathrin-dependent internalization.

In clathrin-dependent endocytosis, the cytoplasmic tails of transmembrane receptors are recognized by the adaptor protein complex 2 (AP-2); the latter then serves as a focal point for the recruitment of clathrin and a wealth of endocytic accessory molecules (3) including (but not limited to) epsin (4), intersectin (5, 6), Eps15 (4), endophilin (7), and the vesiculation protein dynamin (8). However, MHC I and other clathrin-independent cargo are devoid of conventional clathrin-dependent endocytosis signals, and do not interact with classical endocytic accessory proteins. Accordingly, attempts are being made to define specific accessory molecules involved in clathrin-independent endocytosis.

* This work was supported by National Institutes of Health Grants R01GM087455, R01GM074876, and an Institutional Development Award (IDeA) from the National Institute of General Medical Sciences of the National Institutes of Health under Grant number 5P30GM106397. Structured Illumination (SIM) images were obtained and processed at the UNMC Advanced Microscopy Core Facility.
[S] This article contains supplemental videos S1 and S1.
[1] To whom correspondence may be addressed: Dept. of Biochemistry and Molecular Biology and the Fred and Pamela Buffett Cancer Center, The University of Nebraska Medical Center, Omaha, NE 68198. Tel.: 402-559-7559; Fax: 402-559-6650; E-mail: nnaslavsky@unmc.edu.
[2] To whom correspondence may be addressed: Dept. of Biochemistry and Molecular Biology and the Fred and Pamela Buffett Cancer Center, The University of Nebraska Medical Center, Omaha, NE 68198. Tel.: 402-559-7556; Fax: 402-559-6650; E-mail: scaplan@unmc.edu.

[3] The abbreviations used are: MHC, major histocompatibility complex class; TRE, tubular recycling endosome; DGK, diacylglycerol kinase; SIM, structured illumination microscopy; EEA, early endosomal autoantigen; ERC, endocytic recycling compartment; PA, phosphatidic acid; DAG, diacylglycerol; PAP, phosphatidic acid phosphatase.

One novel protein that has recently been added to the list of clathrin-dependent endocytic accessory proteins is diacylglycerol kinase (DGK) δ. Initially identified through genome-wide RNA interference (RNAi) screening for kinases that impact endocytosis (9), it was recently demonstrated that DGKδ localizes to clathrin-coated pits, and its depletion led to impaired internalization of transferrin, a well-characterized clathrin-dependent cargo (10). Indeed, DGKδ interacts with the AP-2α ear domain through a sequence in its catalytic region, and disruption of DGKδ binding to AP-2 the internalization of clathrin-dependent cargo such as epidermal growth factor (10).

DGKδ is a member of a family of 10 mammalian DGKs, all of which catalyze the conversion of diacylglycerol (DAG) to phosphatidic acid (PA) (11). While many of the DGK proteins have not been studied extensively, there is growing evidence that PA impacts receptor internalization (12). PA has also been implicated in the recruitment of proteins such as *M*olecules *I*nteracting with *CAS*L-*L*ike*1* (MICAL-L1) and Syndapin2 to endocytic membranes to promote tubular recycling endosome biogenesis and recycling events (13). Moreover, recent findings indicate that a Type I DGK, DGKα, is essential to support α5β1 integrin recycling and invasive migration (14). Since we were unable to identify an AP-2-binding sequence on DGKα (similar to that of DGKδ (10)), and because integrin trafficking is at least in part mediated through clathrin-independent pathways (15, 16), we hypothesized that DGKα plays a role in the endocytic trafficking of clathrin-independent cargo, such as MHC I.

In this study, we show that DGKα is dispensable for the internalization of MHC I. Somewhat surprisingly, however, DGKα-depletion led to enhanced levels of total and surface-expressed MHC I, resulting from delayed degradation. On the other hand, MHC I recycling to the plasma membrane was impaired in the absence of DGKα. Our findings support a role for DGKα in the regulation of MHC I trafficking, consistent with its function in the conversion of DAG to PA, a step necessary for the generation of MICAL-L1-containing tubular recycling endosomes (TRE).

EXPERIMENTAL PROCEDURES

Cell Lines—HeLa cells were purchased from ATCC. HeLa were grown in DMEM complete media containing 10% FBS, 2 mM glutamine, 100 units/ml penicillin, and 100 units/ml streptomycin.

DNA Constructs—DGKα was cloned from a HeLa cDNA library by PCR amplification with primers (5′-ACGCGTCGACCATGGCCAAGGAGAGGGGCCTAATAAGC-3′, 5′-AAGGAAAAAAGCGGCCGCTTAGCTCAAGAAGCCAAAGAAATTGGTG-3′), and cloned into a pHA-CMV vector (Clontech).

Antibodies and Reagents—Supernatant from the W6/32 hybridoma, producing antibody against MHC I, was previously described (17) and used for immunofluorescence. The mouse monoclonal antibody (HC-10) against MHC I was used for immunoblotting. Other commercial antibodies used were: mouse anti-actin (Novus Biologicals, Inc.), goat anti-mouse horseradish peroxidase (HRP) (Jackson ImmunoResearch Laboratories, Inc.), donkey anti-rabbit HRP (GE Healthcare), Alexa-568 goat anti-mouse, Alexa-488 goat anti-rabbit, and Alexa-647 goat anti-mouse $F(ab)_2$ (Invitrogen), mouse anti-MICAL-L1 (Abnova), rabbit anti-Rab11 (US Biologicals), rabbit anti-HA (Signalway), rabbit anti-EEA1 (Cell Signaling), rabbit anti-caveolin (Cell Signaling), mouse anti-cytochrome *c* (BD Pharmacology), and rat anti-Hsc70 (Stressgene). R59949, propranolol and cycloheximide were purchased from Sigma. 4′,6 diamidino-2-phenylindole (DAPI) was obtained from Invitrogen.

Inhibitor Treatment—To inhibit DGKα or phosphatidic acid phosphatase (PAP) activity, inhibitor treatments were performed as described earlier (13, 18). Briefly, 100 μM (*w*/*v*) of DGKα inhibitor, R59949, was applied for 1 h at 37 °C. 100 μM (*w*/*v*) of the PAP inhibitor, propranolol, was incubated for 30 min at 37 °C.

Immunoblotting—HeLa cells were harvested and lysed on ice for 30 min in lysis buffer containing 50 mM Tris, pH 7.4, 150 mM NaCl, 1% Nonidet P-40, 0.5% sodium deoxycholate, and protease inhibitor mixture (Roche Molecular Biochemicals). Total protein levels in the lysate were then determined by Bio-Rad protein assay (Bio-Rad Laboratories) and normalized for equal protein loading on gels. Protein samples were separated on 10% SDS-PAGE, and detected by immunoblotting with appropriate antibodies.

Densitometry Analysis—Three independent experiments were quantified by densitometry, and analyzed using Image J software. Mean values and standard deviation are presented.

Flow Cytometry and Uptake Assays—HeLa cells were suspended with cell stripper (Mediatech Inc.) and then washed with phosphate-buffered saline (PBS) 3 times. To measure MHC I uptake, the cells were incubated with W6/32 anti-MHCI antibodies for the indicated time at 37 °C. Cells were then subjected to a 1 min acid-strip (0.5 M NaCl, 0.5% acetic acid, pH 3.0) to remove remaining non-internalized MHC I antibody on the cell surface. Cells were fixed with 4% (*v*/*v*) paraformaldehyde in PBS for 10 min. After fixation, the cells were incubated with Alexa-647 goat anti-mouse $F(ab)_2$ in the immunofluorescence staining buffer containing 0.2% saponin (*w*/*v*) and 0.5% BSA (*w*/*v*) in PBS for 1 h at room temperature, followed by 3 washes in PBS. Cells were then subjected to flow cytometry analysis. Values from three independent experiments were normalized. To measure the total/surface level of MHC I at steady-state, HeLa cells were fixed and stained with W6/32 anti-MHC I antibody and then the Alexa-647 goat anti-mouse $F(ab)_2$ in the presence or absence of detergent (saponin).

Immunofluorescence and Recycling Assays—Cells grown on coverslips were fixed with 4% (*v*/*v*) paraformaldehyde in PBS for 10 min as previously described (19). Cells were then incubated with primary antibodies for 1 h at room temperature, followed by three washes in PBS. Cells were incubated with the appropriate fluorochrome-conjugated secondary antibodies in the same staining buffer for 1 h at room temperature. All images were acquired using a Zeiss LSM 5 Pascal confocal microscope (Carl Zeiss) by using a 63× objective with a numerical aperture of 1.4 and appropriate filters. At least 60 cells from three independent experiments were evaluated by Image J for the fluorescence intensity (arbitrary unit) and calculating the area of tubular structures (μm^2).

To measure MHC I recycling, HeLa cells grown on coverslips were incubated with W6/32 anti-MHCI antibodies for 30 min at 37 °C (pulse). The surface-bound and non-internalized MHC I antibody was removed by a 1 min acid-strip (0.5 M NaCl, 0.5%

acetic acid, pH 3.0). The cells were then incubated in complete medium for the indicated times at 37 °C (chase). Cells were fixed, stained with Alexa-568 goat anti-mouse antibody in the absence of detergent for 1 h at room temperature, and subjected to confocal microscopy and Image J analysis.

Transferrin recycling was measured similar to MHC I. HeLa cells grown on coverslips were first pulsed with Transferrin Alexa Fluor® 633 conjugate for 1 h at 37 °C, followed by three washes with PBS, and then incubated in complete medium for 1 h at 37 °C (chase). The amount of transferrin internalized after the pulse, as well as that remaining in the cells after the chase was measured by flow cytometry. The recycling rate of transferrin is presented as the percentage of internalized transferrin remaining in the cell following 1 h chase.

Structured Illumination Microscopy (SIM) Imaging and Data Processing—DMSO- and propranolol-treated cells were fixed and incubated with anti-MICAL-L1 as described for confocal microscopy. SIM images were collected with a Zeiss ELYRA PS.1 illumination system (Carl Zeiss MicroImaging) using a 63× oil objective lens with a numerical aperture of 1.4 at room temperature. Three orientation angles of the excitation grid were acquired for each Z plane, with Z spacing of 110 nm between planes.

SIM processing was performed with the SIM module of the Zen BLACK software (Carl Zeiss MicroImaging). A three-dimensional reconstruction was rendered by a 200-frame rotation series along the Y-axis of processed SIM images, and exported as AVI videos.

Cycloheximide Treatment and MHC I Degradation—Cells grown on 35-mm dishes were treated with 150 μg/ml cycloheximide for 12 h or 24 h. They were then scraped off and lysed for immunoblotting. The amount of remaining MHC I after the indicated times was analyzed by densitometry from three independent experiments. The level of MHC I observed prior to cycloheximide treatment (0 h) was set as 100%.

Coimmunoprecipitation of MICAL-L1—HeLa cells growing in 100-mm dishes were transfected with either HA-DGKα or HA-MARCKS (negative control) using XtremeGENE 9. Cells were then suspended and washed with pre-warmed PBS, and incubated for 1 h in the presence of 100 μM DMSO (control) or 100 μM R59949. Inhibitor-treated cells were lysed with lysis buffer containing 50 mM Tris, pH 7.4, 150 mM NaCl, 0.5% Triton X-100, and 1.8 g/liter iodoacetamide on ice for 1 h. For coimmunoprecipitations, lysates were incubated with anti-MICAL-L1 antibody at 4 °C overnight. Protein L beads were added to the lysate-antibody mix at 4 °C for 4 h. Samples were then washed three times with 0.1% Triton X-100. Proteins were eluted from the protein L beads by boiling in the presence of 4× loading buffer (250 mM Tris, pH 6.8, 8% SDS, 40% glycerol, 5% β-mercaptoethanol, 0.2% bromphenol blue [*w*/*v*]) for 10 min. Eluted proteins were then identified by immunoblotting. HA-DGKα or HA-MARCKS were each detected by anti-HA antibody.

Membrane Fractionation—The isolation of membrane and cytosol fractions of HeLa cells was performed as previously described (20). Cells grown on 100-mm dishes were suspended and homogenized on ice in homogenization buffer containing 25 mM HEPES, 100 mM NaCl, 1 mM EDTA pH 7.4, and protease inhibitor mixture. Cell debris was removed by 1,000 g centrifugation at 4 °C for 10 min. To isolate the membrane and cytosolic fractions, the supernatant was subjected to ultracentrifugation (108,000 × g) at 4 °C for 1 h. The isolated membranes were dissolved in urea buffer (70 mM Tris-HCl, pH 6.8, 8 mM urea, 10 mM *n*-ethylmaleimide, 10 mM iodoacetamide, 2.5% SDS, and 0.1 mM DTT) at 37 °C for 15 min. Immunoblotting was used to detect protein in the fractions. 10% of the cytosolic fraction was loaded onto the gel. Cytochrome *c* served as a specific marker for the cytosol fraction, and caveolin as a membrane fraction marker.

Duolink Proximity Assay—For the Duolink assay (Olink Bioscience), the manufacturer's protocol was followed to visualize two proteins separated by a distance of less than 40 nm (21). HeLa cells grown on coverslips were transfected with GFP-MARCKS (negative control) or GFP-DGKα. After fixation, cells were double- stained with mouse anti-MICAL-L1 and rabbit anti-HA antibody at room temperature for 1 h, followed by the incubation with PLA probe oligonucleotides-conjugated secondary antibody at 37 °C for 1 h. Ligase was then added at 37 °C for an additional 30 min. Polymerase was added for 100 min. at 37 °C for amplification, along with red fluorochrome-labeled primer (complementary to the amplified oligonucleotides). In this case, red dots indicating individual proximity events were counted and plotted from 3 independent experiments.

Transfection and siRNA Treatment—Transfection of HeLa cells for 18 h at 37 °C was performed using X-tremeGENE 9 (Roche Applied Science) according to the manufacturer's protocol.

siRNA treatment was carried out with Oligofectamine (Invitrogen) for 72 h according to the manufacturer's protocol, using 0.3 μM oligonucleotide (Dharmacon). Four specific oligonucleotides (On-Target SMART pool) were directed at human DGKα (5′-GAGAUAGGGCUCCGAUUAU-3′, 5′-CAAUCAAGAUCACCCACAA-3′, 5′-CGACCAGUGUGCCAUGAAA-3′, 5′-ACAGUAGGCUGGAUUCUAG-3′).

RESULTS

The Rate of MHC I Internalization Is Not Regulated by DGKα—MHC I is constantly transported to and from the cell surface, carrying an intracellular-digested peptide, which is presented to cytotoxic T cells, as part of the immune system surveillance. Accordingly, regulation of MHC I trafficking to and from the plasma membrane is a basic requirement for an effective immune response.

DGKδ comprises part of the clathrin-mediated internalization machinery (10). Since MHC I internalizes independently of clathrin and DGKδ, we therefore investigated whether its endocytic itinerary is regulated by a related member of the DGK family, DGKα.

We first measured the internalization rate of MHC I upon depletion of DGKα by siRNA (Fig. 1*A*). HeLa cells were incubated with anti-MHC I antibodies at 37 °C for a short period, followed by a brief acid-strip to remove non-internalized antibody. After fixation, internalized MHC I bound to the antibody was visualized with a secondary antibody (Fig. 1*B*). Because we observed higher levels of MHC I at the cell surface of DGKα-depleted cells (further discussed in Fig. 2, *A*–*F*), the rates of

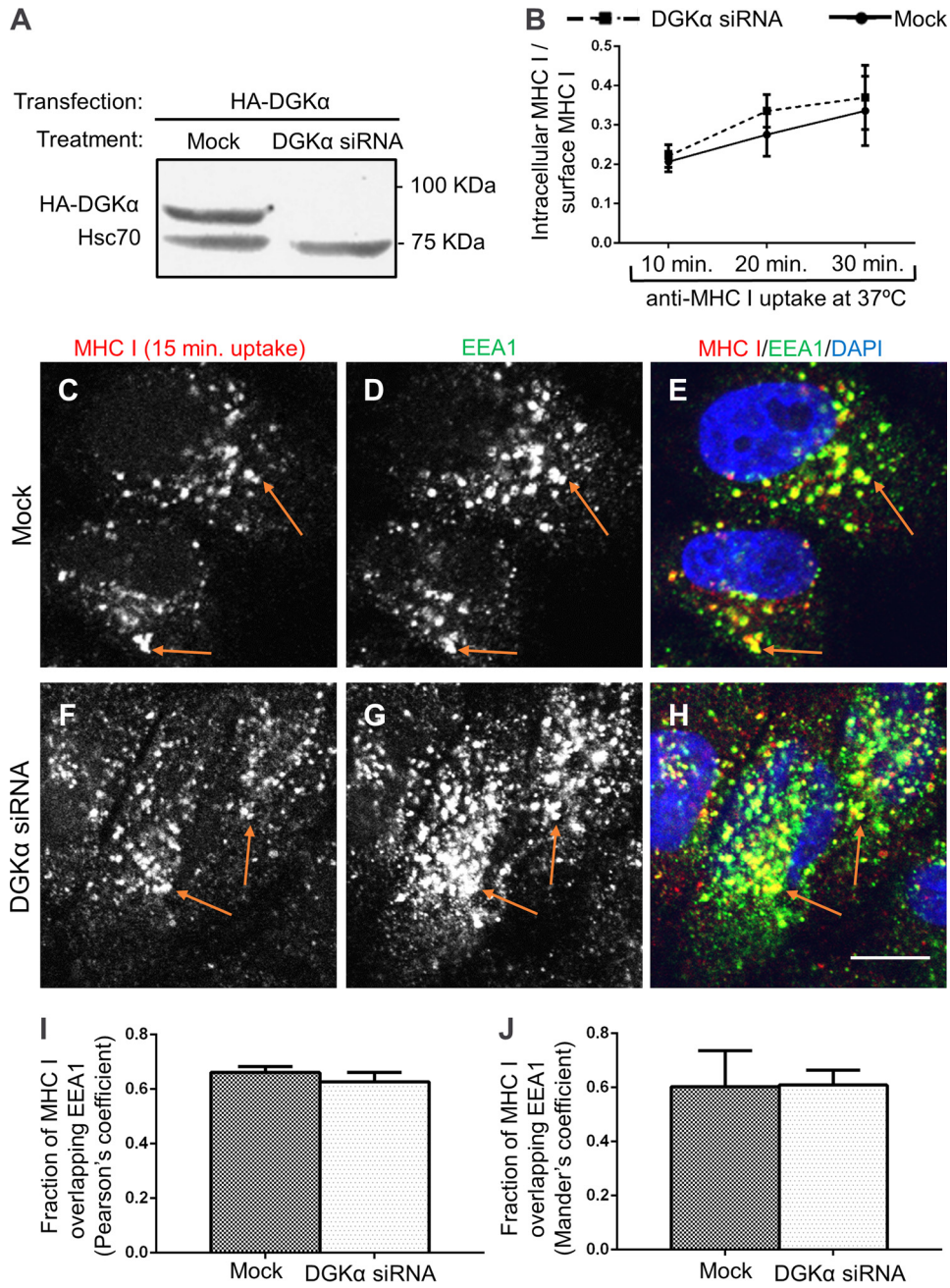

FIGURE 1. **The rate of MHC I internalization is not regulated by DGKα.** *A*, HeLa cells were treated with siRNA against DGKα for 72 h and then transfected with HA-DGKα for 18 h before cell lysis. HA-DGKα expression was measured by immunoblotting with anti-HA. Hsc70 was used as a loading control. *B*, graph depicts flow cytometry analysis of 3 experiments measuring the rate of MHC I internalization. Cells were incubated with W6/32 anti-MHC I for 10, 20, and 30 min at 37 °C, followed by a brief acid-strip to remove non-internalized antibody. After fixation and permeabilization they were stained with Alexa-647 goat anti-mouse $F(ab)_2$. In parallel, the steady-state surface level of MHC I was determined for each treatment by staining with anti-MHC I followed by secondary antibody, both in the absence of saponin. To normalize for different levels of surface MHC I between the treatments (see Fig. 2*A*), the internalization rate was calculated as the ratio between internalized MHC I/steady-state surface MHC I. *C–J*, Mock and DGKα-depleted HeLa cells were incubated with W6/32 mouse anti-MHCI antibody for 15 min at 37 °C, stripped and fixed-permeabilized. Internalized MHC I was detected with Alexa-568 goat anti-mouse. Early endosomes were stained with rabbit anti-EEA1 and Alexa-488 goat anti-rabbit DAPI designates the nuclei. *Orange arrows* exemplify co-localization between MHC I and EEA1, as measured using Image J (*I–J*) and statistically analyzed with Pearson's coefficient (*I*) and Manders' coefficient (*J*). Standard deviation is shown. Bar, 10 μm.

internalized MHC I were normalized to account for this difference. Accordingly, in Fig. 1*B* at 10, 20, and 30 min internalization of MHC I, as detected by flow cytometry, there was no significant alteration. Thus the percent of MHC I molecules internalized from the plasma membrane upon DGKα-depletion remains unchanged.

Shortly after internalization, MHC I-containing vesicles reach sorting endosomes (17). Accordingly, we examined whether internalized MHC I reached sorting endosomes marked by the early endosomal autoantigen 1 (EEA1), upon DGKα-siRNA treatment. To this aim, either Mock-treated or DGKα-depleted HeLa cells were incubated with anti-MHC I antibody for 15 min at 37 °C to monitor internalization, before being acid-stripped and fixed-permeabilized.. The co-stain of internalized MHC I and EEA1 was assessed (Fig. 1, *C–H*) and quantified by Image J with two different statistical tests

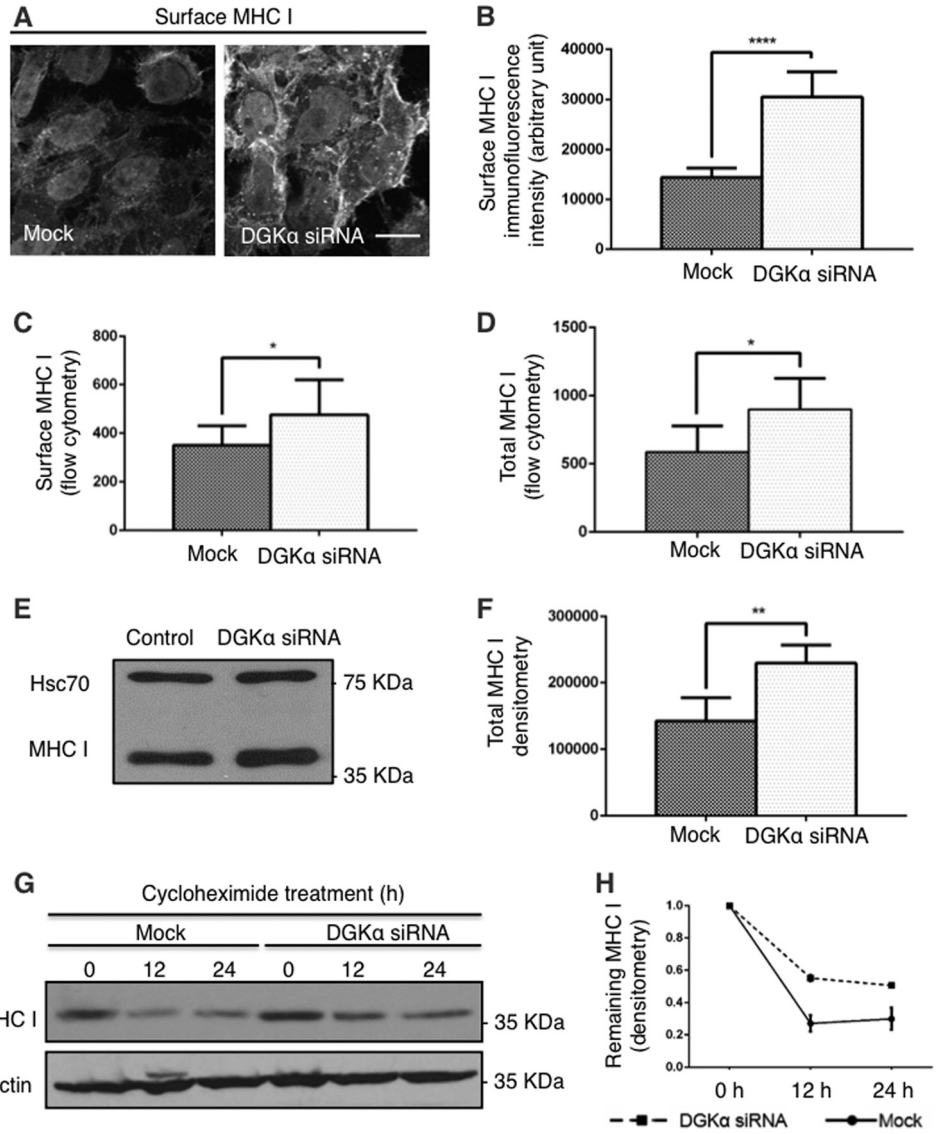

FIGURE 2. **DGKα controls the half-life of MHC I.** *A–C*, surface level of MHC I for Mock and DGKα-knock-down cells was measured by immunofluorescence staining (*A*), and quantified by Image J in *B* and by flow cytometry (*C*). Briefly, Mock and DGKα knock-down cells were fixed and stained with anti-MHC I and secondary antibody in the absence of permeabilizing detergent. *D–F*, total cellular MHC I protein from Mock- and DGKα-depleted cells was measured by flow cytometry (*D*) with anti-MHC I and secondary antibody in the presence of saponin, and by immunoblotting (*E*; Hsc70 serves as a loading control). *F*, graph depicts densitometry analysis of three independent experiments as in *E*. *G*, 150 μg/ml cycloheximide was applied to HeLa cells for 0, 12, and 24 h prior to lysis. Immunoblotting of total cellular MHC I protein was done with anti-MHCI antibody. *H*, densitometry analysis of three independent experiments as in *G* is shown with standard deviation. *, $p < 0.05$; **, $p < 0.0025$; ****, $p < 0.0001$. Bar, 10 μm.

(Pearson's and Manders' coefficients, Fig. 1, *I–J* accordingly). Both analyses indicate that the ablation of DGKα did not significantly alter the normal influx of MHC I into sorting endosomes.

A longer internalization period (30 min) led to a decreased co-localization between MHC I and EEA1 in both Mock and DGKα-siRNA-treated cells (data not shown), suggesting that the exit of MHC I-containing vesicles from early endosomes was similarly unaffected by DGKα-depletion. Taken together, our data suggest that MHC I internalization and its access to sorting endosomes are not regulated by DGKα.

DGKα Controls the Half-life of MHC I—Antigen presentation to lymphocytes by MHC I directly depends on its level at the plasma membrane. Having seen that DGKα does not partake in MHC I internalization, we now turned to inquire whether DGKα affects MHC I partitioning at the plasma membrane by knocking down DGKα and measuring cell-surface residing MHC I.

Surprisingly, the surface staining intensity of MHC I dramatically increased in DGKα-depleted cells, as shown by immunofluorescence of non-permeabilized cells (Fig. 2*A*, *right panel*) compared with Mock-treated cells (Fig. 2*A*, *left panel*). Image J quantification of the fluorescence intensity from three independent experiments (Fig. 2*B*) revealed nearly a 2-fold increase in the amount of MHC I residing on the cell surface of DGKα-depleted cells. Likewise, flow cytometry analysis under similar conditions confirmed increased levels of MHC I on the plasma membrane in DGKα-depleted cells, although to a lesser extent than that measured by immunofluorescence (Fig. 2*C*, 25% increase).

The elevation of surface-MHC I in DGKα-depleted *versus* Mock-treated cells was mirrored by an overall increase in the total cellular MHC I, as observed by two lines of experiments: First, flow cytometry measurements (in Fig. 2*D*) of cells permeabilized with saponin, revealed that siRNA knock-down of DGKα caused a similar elevation in total MHC I to that observed on the cell surface (~33%). Second, immunoblotting also showed a significant increase in total MHC I upon DGKα knock-down (Fig. 2*E*; Hsc70 serves as a loading control). Fig. 2*F* depicts densitometric quantification of 3 separate immunoblotting experiments, as done in Fig. 2*E*).

We hypothesized that the total MHC I level increased in the absence of DGKα due to impaired MHC I degradation. To test this hypothesis, we assessed the rate of MHC I degradation by following the cellular MHC I level over time upon inhibition of *de novo* protein synthesis with cycloheximide. Immunoblotting (Fig. 2*G*, *upper gel*) and densitometry analysis of 3 similar experiments in Fig. 2*H*, showed that ~70% of MHC I underwent degradation in the first 12 h in Mock-treated cells, with little additional degradation at 24 h. In contrast, in DGKα-depleted cells, only ~40% of MHC I was degraded at 12 and 24 h. We conclude, therefore, that there is mis-sorting of MHC I in DGKα-depleted cells at a post sorting-endosome stage that causes its inefficient degradation. This, in turn, leads to its accumulation both inside the cell and at the plasma membrane.

DGKα Depletion Interferes with MHC I Trafficking to the Recycling Compartment and Delays Its Recycling—To investigate which post-endosomal trafficking steps are regulated by DGKα, we followed the intracellular itinerary of internalized MHC I over time using a pulse-chase immunofluorescence-based assay. We incubated cells with anti-MHC I antibody for 30 min at 37 °C (pulse) followed by a 1 min acid-strip to remove non-internalized antibody, and then chased in complete media for 30 min, 1 h, and 2 h at 37 °C. Previous works demonstrated that within 1–2 h chase most internalized MHC I reaches the recycling compartment in HeLa cells (17, 19, 22, 23). Thus at shorter time points, as we show here in Fig. 3, *A* and *D*, (30 min pulse and 30 min chase), scattered vesicles containing MHC I were visible in both Mock- and siRNA-treated cells. Some MHC I could be observed starting to concentrate in the perinuclear area. This scattered pattern is consistent with the MHC I distribution obtained after the short 15 min uptake described in Fig. 1, *C*–*H*, and its association with sorting endosomes. Note that upon DGKα-loss, a greater total *amount* of MHC I uptake was recorded (~2-fold more), although the normalized rate of uptake was relatively unchanged (Fig. 1*B*). This likely results from the ~2-fold increased level of surface-expressed MHC I (observed in Fig. 2).

On the other hand, at 1 h and 2 h chase in Mock-treated cells, the MHC I reached a compact and bright perinuclear area (Fig. 3, *B* and *C*; *arrows*) corresponding to the Endocytic Recycling Compartment (ERC). For DGKα-depleted cells, however (Fig. 3, *E* and *F*), after either a 1 h or 2 h chase, MHC I maintained its scattered distribution in the cell periphery. Only at a later time point (3 h; data not shown), MHC I began to concentrate at the perinuclear area, suggesting a delay in MHC I trafficking to the ERC upon DGKα depletion.

The delayed delivery of MHC I to the ERC in DGKα-knock-down cells prompted us to hypothesize that MHC I recycling back to the plasma membrane might be similarly delayed. To test this, we used an immunofluorescence-based assay to measure the re-appearance (recycling) of MHC I at the plasma membrane. HeLa cells were incubated with anti-MHC I antibodies for 30 min at 37 °C and briefly acid-stripped. Following 3 h chase in complete media, anti-MHC I returning to the plasma membrane was monitored with a secondary antibody in the absence of detergent (Fig. 3*G*). Surface anti-MHC I was measured by Image J. To normalize the difference in surface MHC I levels observed at the starting point (see Fig. 2, *A*–*C*), a parallel set of permeabilized cells was used to measure the *total* MHC I level. Thus, recycled MHC I was calculated as a portion of the total pool. In Mock-treated cells, ~40% of MHC I returned to the cell surface within a 3-h chase, while in DGKα knock-down cells, only ~10% returned (Fig. 3*G*). This supports the notion that DGKα affects MHC I recycling.

On the other hand, no affect of DGKα knock-down was observed for transferrin recycling (Fig. 3*H*). However, β1-integrin, whose recycling is regulated by DGKα (17) and may be internalized either via clathrin (24, 25) or independently of clathrin-coated pits (26), also displayed increased surface levels upon DGKα-depletion (Fig. 3*K*). However, unlike MHC I, no changes in total cellular β1-Integrin were recorded (Fig. 3, *I* and quantified in *J*), suggesting that MHC I and β1-integrins have different intracellular degradation routes.

DGKα Is Required for the Biogenesis of Tubular Recycling Endosomes—In search of a mechanism to explain the involvement of DGKα in MHC I recycling, we turned to the enzymatic reaction catalyzed by DGKα; the generation of phosphatidic acid (PA) by phosphorylating diacylglycerol (DAG) (Fig. 4*F*). Having previously described a role for PA in the biogenesis of TRE (13), we next questioned whether DGKα is also essential for the biogenesis of TRE, which are required for MHC I recycling.

To visualize TRE by immunofluorescence we used MICAL-L1, previously described as an endogenous marker for these tubular structures (27). MICAL-L1-decorated TRE are typically detected in 50% of HeLa cells during interphase, and they are depicted in a field of Mock-treated cells in Fig. 4*A* (and inset). In contrast, when DGKα was depleted, TRE appeared as significantly shorter tubular structures (Fig. 4*B*, see *inset*). Upon DGKα knock-down, where synthesis of PA is compromised, we sought to preserve PA levels by preventing its catabolism. Propranolol is an inhibitor of phosphatidic acid phosphatase (PAP), which dephosphorylates PA to generate DAG (illustrated in Fig. 4*F*). Thus, DGKα- depleted cells were incubated with propranolol for 30 min at 37 °C. As shown in Fig. 4*D*, arresting PA catabolism with propranolol, rescued TRE formation, giving rise to elaborate MICAL-L1-decorated tubular structures (compare supplemental video S2 to supplemental video S1). Indeed, propranolol treatment similarly induced TRE formation in Mock-treated cells (Fig. 4*C*).

TRE formation was quantified by measuring MICAL-L1-containing tubular area per cell by Image J analysis. Three different experiments (done as in Fig. 4, *A*–*D*) are plotted in Fig. 4*E* (analyzing 60 cells taken from each treatment). We found that

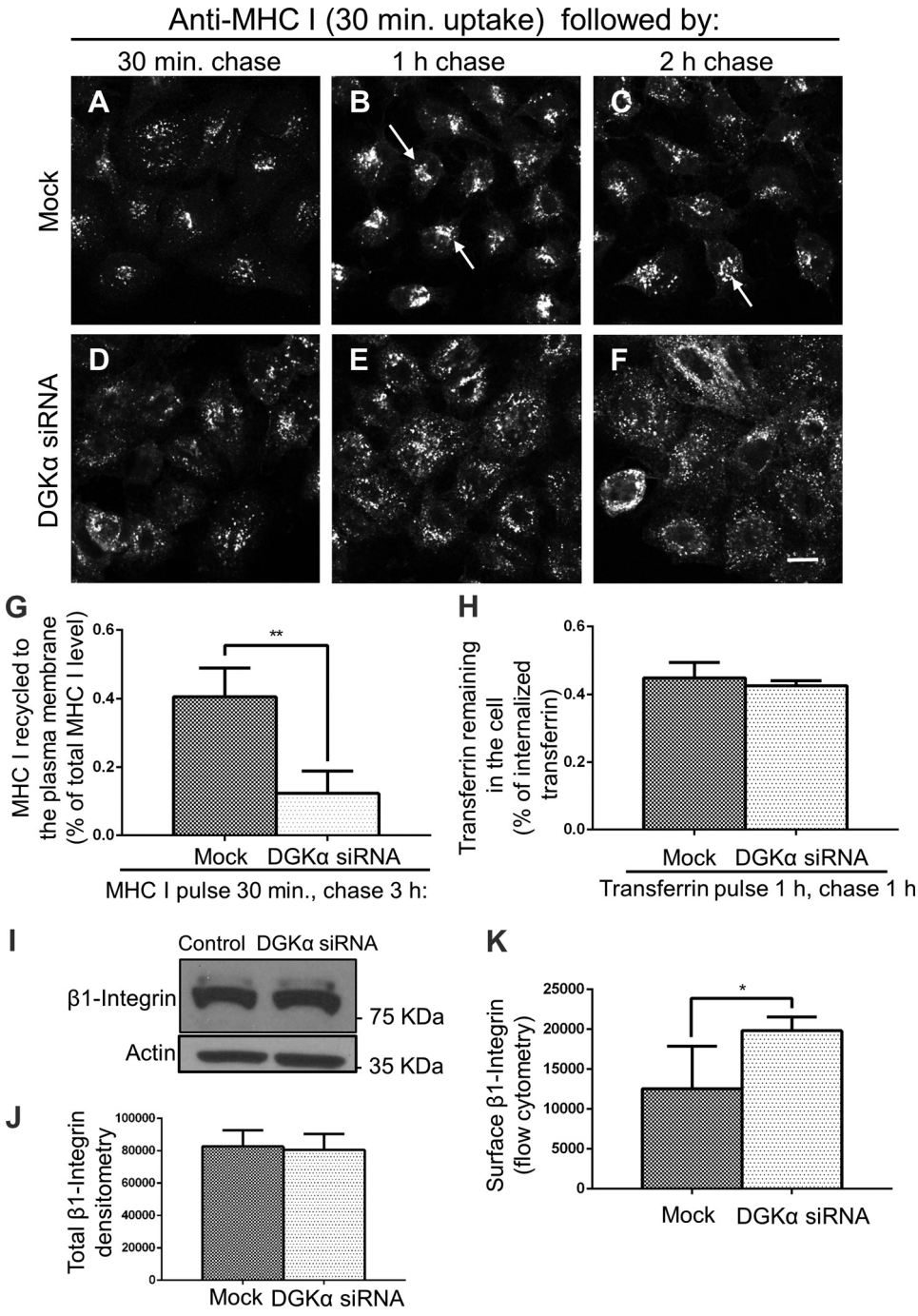

FIGURE 3. **DGKα-depletion interferes with MHC I trafficking to the recycling compartment and recycling to the plasma membrane.** *A–F*, Mock and DGKα-depleted HeLa cells were incubated with anti-MHC I antibody for 30 min at 37 °C (pulse), stripped, and chased in complete medium for 30 min, 1 h, and 2 h at 37 °C, followed by a second strip and fixation-permeabilization. MHC I remaining in the cell was detected with Alexa-568 goat anti-mouse. *Arrows* point to MHC I concentrated in the ERC. *G*, quantification of immunostained MHC I that re-appeared at the PM (underwent recycling). Mock and DGKα-depleted cells were pulsed as in *A–F*, then chased for 3 h, followed by fixation. The cells were stained with Alexa-568 goat anti-mouse antibody in the absence of detergent. The total MHC I was measured in parallel with fixed cells incubated with anti-MHC I in the presence of detergent. The return of MHC I to the cell surface (following 3-h chase) was calculated as a portion of the total MHC I. 120 cells from three independent experiments were analyzed with Image J. *H*, graph depicts flow cytometry analysis of three experiments measuring the rate of transferrin recycling. Mock- and DGKα-depleted HeLa cells were incubated with Transferrin Alexa Fluor® 633 conjugate for 1 h at 37 °C (pulse), and chased in complete medium for 1 h at 37 °C. Cells were then fixed and subjected to flow cytometry. *I–J*, total level of β1-Integrin for Mock and DGKα-knock-down cells was measured by immunoblotting. Densitometry analysis of three independent experiments as in *A* is shown in *B* with standard deviation. *K*, surface level of β1-integrin for Mock and DGKα-knock-down cells was measured by flow cytometry with anti-β1-integrin and appropriate secondary antibody staining in the absence of permeabilizing detergent. Statistical analysis was performed with data from three independent flow cytometry experiments. Shown is standard deviation. *, $p < 0.05$; **, $p < 0.0025$.

the MICAL-L1-containing tubular area averaged 10 μm^2/Mock-treated cells, while DGKα-depleted cells had only 5 μm^2/cell. In the DGKα-depleted cells that received propranolol treatment, TRE area reached as high as 40 μm^2/cell, suggesting that: (I) other enzymes, such as PLD and LPAT may allow generation of basal levels of PA in the absence of DGKα, and (II)

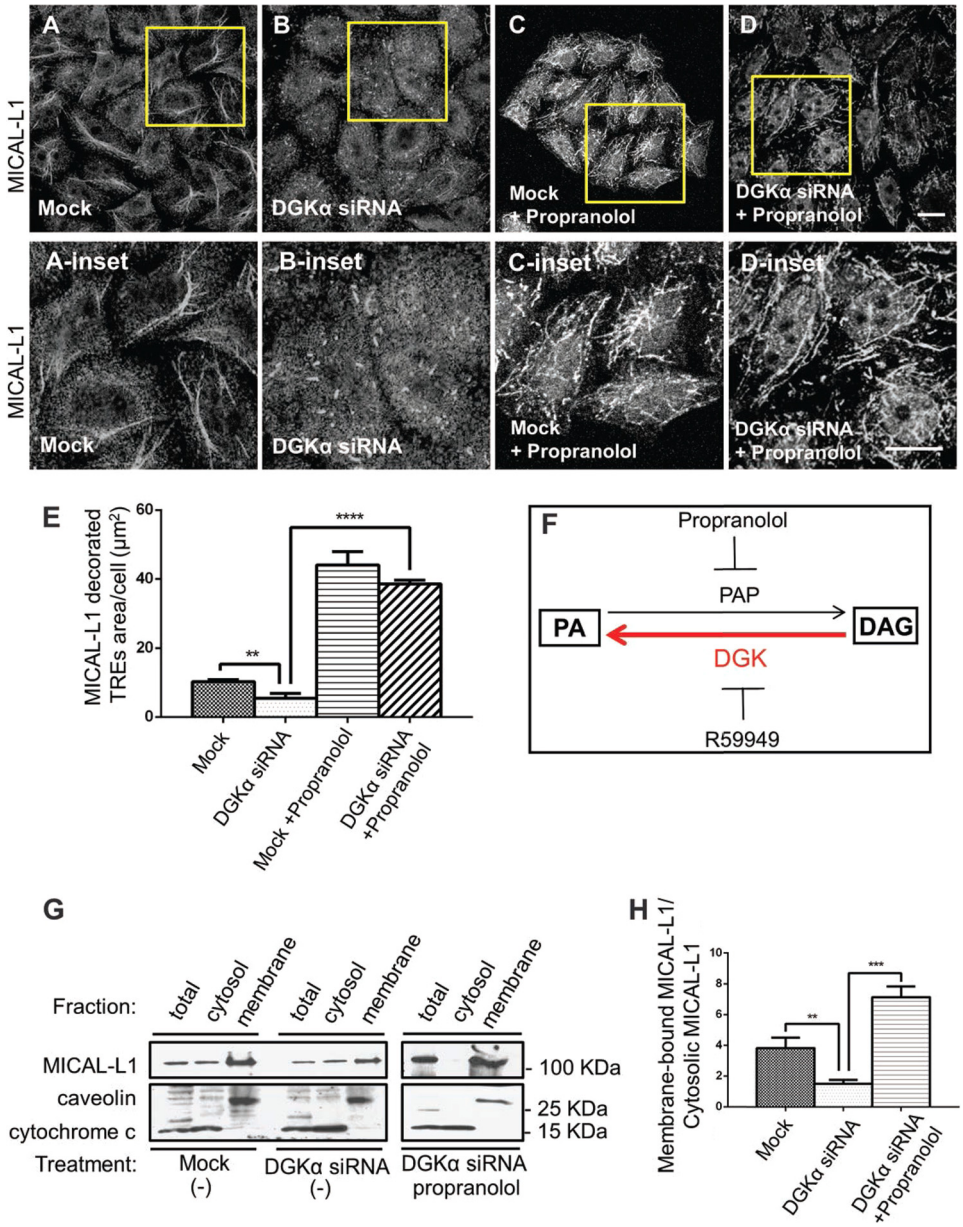

FIGURE 4. **DGKα is required for the biogenesis of tubular recycling endosomes.** *A–D*, morphology of TRE was assessed by immunostaining with the endogenous TRE marker, MICAL-L1. HeLa cells were treated with Mock (*A*) or DGKα-siRNA (*B*) for 72 h. *C*, Mock- or *D*, DGKα-siRNA-treated cells were also incubated with 100 μM propranolol, a phosphatidic acid phosphatase (PAP) inhibitor, for 30 min at 37 °C (*A-B* were treated with DMSO). After fixation, cells were stained with anti-MICAL-L1 antibodies and Alexa-568 goat anti-mouse secondary antibody. *Yellow boxes* depict the insets shown below. *E*, image J analysis of *A–D*; MICAL-L1 area per cell, using 60 cells from three independent immunofluorescence staining experiments. *F*, schematic diagram illustrating the function of DGK, PAP, and their corresponding inhibitors. *G*, HeLa cells were treated as in *A–C*, and then homogenized. Cytoplasmic and membrane fractions were separated by ultracentrifugation. The entire membrane fraction and 10% of the cytosolic fractions were separated on SDS-PAGE, and MICAL-L1 was detected by immunoblotting. *H*, densitometry analysis from 3 independent membrane fractionation experiments (as done in *F*) is shown as the ratio of membrane-bound MICAL-L1 to cytosolic MICAL-L1. Error bars represent standard deviation. **, $p < 0.0025$; ***, $p < 0.0005$; ****, $p < 0.0001$. Bars, 10 μm.

PAP inhibition by propranolol effectively caused PA accumulation, possibly due to a rapid *in vivo* turnover of PA to diacylglycerol by PAP (see "Discussion").

The requirement of PA for TRE formation was further tested biochemically in Fig. 4*G*. Endogenous membrane-bound MICAL-L1 (representing intact TRE) was isolated by homogenization and ultracentrifugation. As described under "Experimental Procedures," either Mock-treated or DGKα-siRNA-treated cells (in the presence or absence of propranolol), were homogenized and subjected to ultracentrifugation to separate supernatant containing cytosolic proteins from the pellet containing membrane-bound proteins. The level of endogenous MICAL-L1 in each fraction was detected by immunoblotting; caveolin was used as a membrane-bound control, whereas cytochrome *c* was used as a cytosolic protein marker (Fig. 4*G*). Note that the band representing caveolin shifted upward in the membrane fraction compared with total and cytosol fractions, possibly due to the use of urea to solubilize the membrane sample.

As shown in Fig. 4*G* (*upper panel*), compared with Mock-treated cells, membrane-bound MICAL-L1 decreased substantially upon DGKα-depletion (10% of the cytosolic fraction was loaded). This is in line with our immunofluorescence staining,

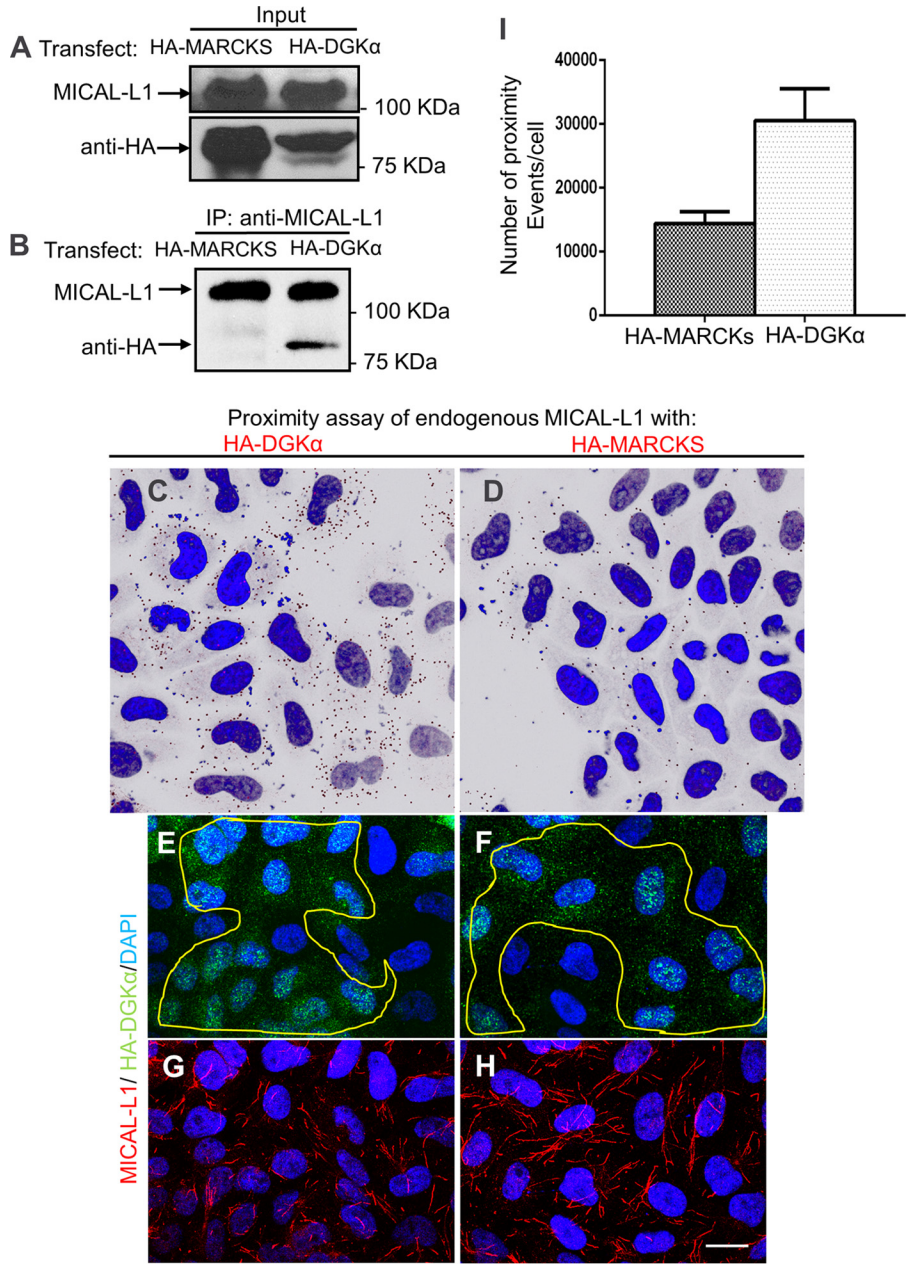

FIGURE 5. **DGKα forms a complex with MICAL-L1.** DGKα and MICAL-L1 co-immunoprecipitate. *A*, HA-MARCKS (negative control) and HA-DGKα-transfected cells were lysed and blotted with anti-HA. *B*, in the same lysates, endogenous MICAL-L1 was pulled-down with anti-MICAL-L1 and eluted. Eluates were immunoblotted with anti-HA and anti-MICAL-L1. *C–H*, micrographs depicted show representative data from proximity ligation assays. Cells grown on coverslips were transfected with GFP-DGKα or HA-MARCKS (negative control). Duolink (proximity ligation) assay was performed using mouse anti-MICAL-L1 and rabbit anti-GFP. Dark dots in *C–D* indicate proximity (<40 nm) between MICAL-L1 and the HA-tagged protein. *E–F*, the same cells were also immunostained with anti-HA, to show similar degrees of transfection. *G* and *H*, endogenous MICAL-L1 was immunostained to display TRE morphology. *I*, number of proximity ligation events from 3 independent experiments (as done in *C–D*) was counted by Image J and plotted with standard deviation. Bar, 10 μm.

which showed diminished and dramatically shortened TRE under these conditions (compare with Fig. 4, *A* and *B*). In contrast, when the DGKα-depleted cells were treated with propranolol (Fig. 4*G*, *right upper panel*), almost all of the MICAL-L1 shifted to the membrane fraction, reflecting the increase of MICAL-L1-decorated TRE observed in Fig. 4*D*.

Densitometry measurements of 3 fractionation experiments (as in Fig. 4*G*), were used to compare the ratio of MICAL-L1 in the membrane *versus* cytosolic fraction (Fig. 4*H*). As calculated, upon DGKα-depletion, membrane-bound MICAL-L1 comprised less than a half of its normal membrane-association in Mock-treated cells. The extent of this reduction is similar to the immunofluorescence-based analysis in Fig. 4*E* (*left* and *middle bars* on the graph). Propranolol treatment caused a massive recruitment of MICAL-L1 to membranes, as evidenced in morphologic and biochemical assessments (Fig. 4, *C–E*, *G–H*). Taken together, DGKα is important for TRE formation and maintenance, possibly by providing a means for local PA elevation in membranes.

DGKα Forms a Complex with MICAL-L1—Having shown that DGKα is essential for the recruitment of MICAL-L1 onto tubular membranes, we next hypothesized that DGKα interacts

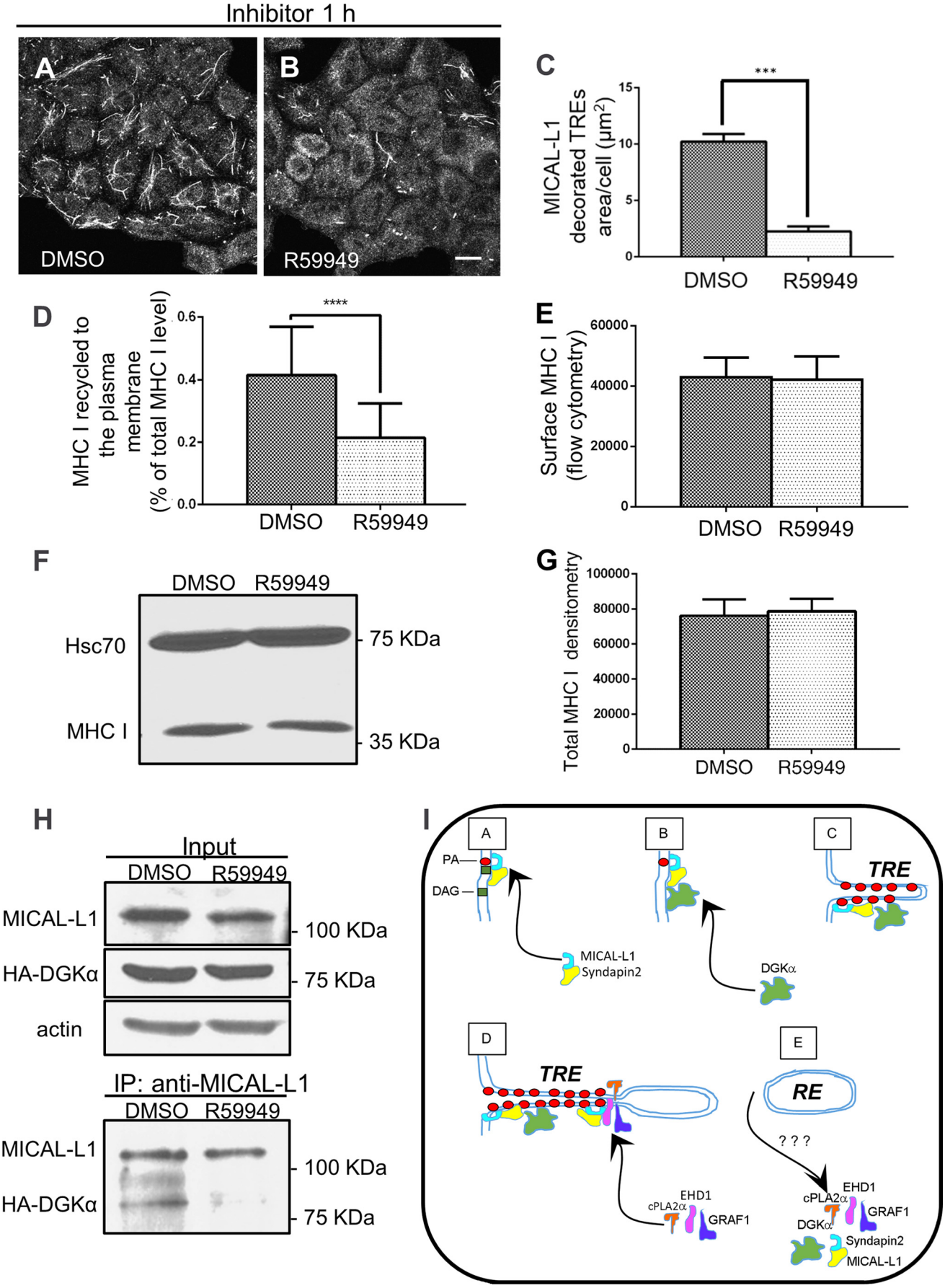
Inhibitor 1 h
A
DMSO
B
R59949
C
MICAL-L1 decorated TREs area/cell (μm²)
***
DMSO
R59949
D
MHC I recycled to the plasma membrane (% of total MHC I level)
****
DMSO
R59949
E
Surface MHC I (flow cytometry)
DMSO
R59949
F
DMSO R59949
Hsc70
75 KDa
MHC I
35 KDa
G
Total MHC I densitometry
DMSO
R59949
H
Input
DMSO R59949
MICAL-L1
100 KDa
HA-DGKα
75 KDa
actin
IP: anti-MICAL-L1
DMSO R59949
MICAL-L1
100 KDa
HA-DGKα
75 KDa
I
A
PA
DAG
MICAL-L1
Syndapin2
B
DGKα
C
TRE
D
TRE
E
RE
???
EHD1
cPLA2α
GRAF1
EHD1
cPLA2α
GRAF1
DGKα
Syndapin2
MICAL-L1

with MICAL-L1. Although these two proteins partition into cytosolic *and* membranous fractions, we assumed that an interaction between them might occur on membranes. To address their potential association we performed co-immunoprecipitation and *in vivo* co-staining. For co-immunoprecipitation, HA-DGKα or HA-MARCKS-transfected cells (control) were lysed (Fig. 5*A*, *upper panel*), and endogenous MICAL-L1 was pulled-down with specific antibodies. As demonstrated in Fig. 5*B*, HA-DGKα, but not HA-MARCKS, was immunoprecipitated by MICAL-L1. This association appears to be indirect, as it could not be detected by a selective yeast two-hybrid assay (data not shown).

To assess whether DGKα and MICAL-L1 associate *in vivo*, a proximity ligation assay (Duolink®) was performed. This assay detects *in situ* proximity (<40 nm) between two proteins (21) and unlike conventional immunofluorescence methods, such interactions can be detected even when a major portion of the protein is cytoplasmic (cytosolic DGKα) .

Cells transfected with similar expression levels of HA-DGKα (Fig. 5, *C*, *E*, and *G*) or HA-MARCKS (negative control: Fig. 5, *D*, *F*, and *H*) were fixed and processed for the proximity assay according to the manufacturer's protocol, using primary antibodies: mouse anti-MICAL-L1 to detect endogenous MICAL-L1 and rabbit anti-HA. Oligonucleotides conjugated to secondary antibodies, underwent ligation if residing <40 nm apart from each other. A specific fluorescent label detected such ligation events (seen as *dark dots* in Fig. 5, *C–D*, nuclei are stained with DAPI).

A significant number of proximity events (dots) were observed in HA-DGKα transfected cells (Fig. 5*C*), compared with the HA-MARCKS-transfected negative control (Fig. 5*D*). Note that these events do not necessarily align with the membrane tubules, possibly because they represent a small fraction of the total MICAL-L1-DGKα interactions. It is also possible that amplification of the signal precludes amplification from closely neighboring interaction pairs. Image J quantification of three independent proximity assays is summarized in Fig. 5*I*, indicating that DGKα and MICAL-L1 are in close proximity *in vivo*. Fig. 5, *E–F* are controls, showing equal levels of transfection for both HA-tagged proteins, whereas the MICAL-L1 immunostaining (*G–H*) demonstrates the efficiency of the DGKα-depletion (with shorter and fewer TRE observed in *G*).

The Biogenesis of Tubular Recycling Endosomes Requires the Activity of DGKα—We show here that DGKα is required for the biogenesis of TRE and that it partially localizes and associates with MICAL-L1-containing TRE *in vivo*. We next investigated whether PA was directly required for the association between MICAL-L1 and DGKα. To this aim, we used the diacylglycerol kinase inhibitor, R59949, to arrest PA production (illustrated in Fig. 4*F*). As shown in Fig. 6, *A* and *B*, upon 1 h treatment with R59949, the number and size of MICAL-L1-containing TRE dropped substantially. Quantification of the mean square area of TRE from three independent experiments is summarized in Fig. 6*C*. This loss of TRE is similar to the one observed upon DGKα-siRNA treatment (see Fig. 4, *A* and *B*).

We next posited that similar to DGKα-depletion, acute R59949 treatment would impair MHC I recycling to the plasma membrane. As demonstrated, there was a significant delay in MHC I recycling (Fig. 6*D*).

Because long-term DGKα-depletion increases total cellular MHC I levels as well as MHC I levels on the plasma membrane, we next asked whether acute R59949 treatment (1 h) causes similar effects. As demonstrated, no increase in total MHC I was observed (Fig. 6, *F* and quantified in *G*). Likewise, cell surface MHC I levels were also unaffected by R59949 treatment (Fig. 6*E*).

Under these conditions of DGKα-depletion and subsequent decrease of MICAL-L1-containing TRE, we now asked whether DGKα and MICAL-L1 continue to associate. As shown in Fig. 6*H*, although the DGKα inhibition did not alter the MICAL-L1 protein level substantially (upper panel), co-immunoprecipitation indicated that impaired PA generation resulted in the loss of interaction between MICAL-L1 and DGKα (Fig. 6*H*, *lower panel*). Taken together, we propose that the activity of DGKα is required for TRE formation and MHC I recycling

DISCUSSION

There is increasing evidence that local concentrations of PA within the membranes of cellular organelles impact trafficking through the endocytic pathways. For example, PA affects receptor internalization (12), and it is required both for the generation of TRE and the recycling of receptors to the plasma membrane (13). To date, however, little is known about the mechanisms that regulate the temporal generation of local PA concentrations.

FIGURE 6. **The biogenesis of tubular recycling endosomes requires the activity of DGKα.** *A* and *B*, cells grown on coverslips were treated with either DMSO or 100 μM R59949 (DGK inhibitor) for 1 h at 37 °C, fixed-permeabilized, and then stained with anti-MICAL-L1. *C*, mean square area of TRE-localized endogenous MICAL-L1, taken from three independent experiments (from the experiments depicted in *A* and *B*), was measured with Image J and plotted with standard deviation, *D*, quantification of immunostained MHC I that re-appeared at the PM (underwent recycling). DMSO- and R59949-treated cells were pulsed with anti-MHC I antibody for 30 min at 37 °C, then chased for 3 h, followed by fixation. The cells were stained with Alexa-568 goat anti-mouse antibody in the absence of detergent. The total MHC I was measured in parallel with fixed cells incubated with anti-MHC I in the presence of detergent. The return of MHC I to the cell surface (following 3 h chase) was calculated as a portion of the total MHC I. 120 cells from three independent experiments were analyzed with Image J. *E*, surface level of MHC I for DMSO- and R59949-treated cells was measured by flow cytometry. *F*, total MHC I level of DMSO- or R59949-treated cells was measured by immunoblotting with anti-MHC I (HC10). Hsc70 was used as a loading control. *G*, graph depicts densitometry analysis of three independent experiments as in *D*. Shown is standard deviation. *H*, impaired PA production results in the loss of interaction between MICAL-L1 and DGKα. HA- DGKα transfected cells, growing on 100-mm dish were incubated with either DMSO or 100 μM R59949 for 1 h at 37 °C, and lysed (see *input upper panel* in *H*; anti-actin is a loading control). Lysates were co-immunoprecipitated with anti-MICAL-L1 antibodies (*lower panel* in *H*), and immunoblotted with anti-HA, and anti MICAL-L1. *I*, proposed model depicting the role of DGKα in TRE biogenesis. DGKα is recruited onto membranes through its interaction with a complex containing MICAL-L1. This leads to further generation of PA, and further recruitment of MICAL-L1, which serves as a membrane hub. Its association with the BAR-containing protein, Syndapin2, and the local enrichment of PA culminate in elongation of the membrane into a tubular endosome. Potential "vesiculators" such as EHD1, GRAF1, and cPLA2α are then recruited by MICAL-L1 and form a constriction site, ultimately leading to scission/budding of a transport vesicle. ***, $p < 0.0005$; ****, $p < 0.0001$. Bar, 10 μm.

Several pathways have been described that lead to the generation of PA in mammalian cells. First, lysophosphatidic acid can be converted to PA by the transfer of an acyl chain by enzymes known as lysophosphatidic acyl transferases (LPAT), and acylglycerol phosphate acyltransferases (AGPAT) (reviewed in Ref. 28). Phospholipase D can also generate PA, by removing the head group of glycerphospholipids such as phosphatidylcholine (29). In addition, the phosphorylation of diacylglycerol can lead to conversion to PA through the action of diacylglycerol kinases (reviewed in Ref. 11).

In this study, we have focused on the role of DGKα in the trafficking of MHC I, a receptor that is typically internalized in a clathrin-independent manner, for several reasons. First, of the 10 DGKs, DGKα is widely expressed in a variety of cell types, including fibroblasts, T lymphocytes, endothelial cells, and various stem cells (11). Second, whereas the Type II DGKs (δ, η, and κ) contain Adaptor Protein-2 (AP-2) α-ear binding sites, DGKα lacks these motifs, rendering it more likely to regulate clathrin-independent cargo. In addition, a recent study demonstrated that DGKα plays a role in integrin recycling and cell invasiveness, by tethering the Rab11 effector, Rab-coupling protein (RCP), to pseudopodal tips (14).

We have demonstrated that DGKα-depletion affects the intracellular itinerary of MHC I. While the net amount of MHC I that was internalized in the absence of DGKα was increased ~2-fold, the rate at which individual MHC I molecules were internalized did not increase. The greater number of internalized MHC I molecules likely resulted from an increase in the amount of MHC I residing at the plasma membrane. This increase was concurrent with a similar increase in the total cellular level of MHC I that accumulated in the absence of DGKα. Moreover, from previous studies, we have seen that delays in receptor recycling are transient effects, and cells have mechanisms to overcome these delays over time (30, 31).

How do we reconcile increased expression of MHC I at the plasma membrane, yet delayed recycling upon DGKα knockdown? We hypothesize that over a 72-h period (of DGKα-depletion) there is a form of compensation that essentially allows the cell to arrive at a new steady-state equilibrium. However, this catch-up would only occur chronically over a long period of time (days). Indeed, acute recycling, as measured by a short recycling assay (minutes to hours), even once this equilibrium has been reached, demonstrates that recycling is nonetheless impaired.

In support of this notion is our data demonstrating that the acute DGK inhibitor, R59949, inhibits MHC I recycling (and TRE biogenesis), but neither increases *total* nor plasma membrane MHC I (Fig. 6). These data provide additional evidence that DGKα regulates MHC I recycling acutely, while having a more complex affect on MHC I trafficking when its function is impaired for longer periods of time. Thus in cases of chronic loss of function, in addition to regulating MHC I recycling, DGKα might also affect MHC I trafficking at an earlier step in the pathway.

While further studies will be needed to address the potential role of DGKα upstream of recycling endosomes, depletion of this enzyme had the most dramatic effect on MHC I recycling, causing an acute delay in the return of the receptor to the plasma membrane. Since we have recently demonstrated that TRE biogenesis is required for normal receptor recycling, and PA is an essential lipid needed for the initiation of TRE biogenesis (13), we proposed that DGKα activity facilitates TRE formation and recycling by the conversion of diacylglycerol to PA. Our data demonstrate that DGKα-depletion leads to the loss of MICAL-L1-containing TRE, and that this effect could be blocked by treatment with propranolol, an inhibitor of the PA phosphatase enzyme that converts PA to diacylglycerol.

Because DGKα is mostly localized to the cytoplasm, its effective recruitment to membranes is key to its activity in the cell. Our co-immunoprecipitations and proximity ligation assays provide evidence that DGKα forms a complex with MICAL-L1, leading us to speculate that in its capacity as a membrane hub (32), MICAL-L1 recruits DGKα to recycling endosomes. As such, we envision a mechanism in which the generation of PA by DGKα serves as a positive feedback loop for recruitment of more MICAL-L1 and DGKα, spurring additional local PA generation that facilitates TRE biogenesis (see working model in Fig. 6*I*). In this model (*A*), MICAL-L1 and Syndapin2, which bind with high selectivity to PA (13), are recruited onto membranes containing DAG and some PA. (*B*) DGKα then associates with the membrane, forming a possible complex with MICAL-L1. (*C*) local generation of additional membrane-embedded PA further shapes membrane elongation into TRE that contain cargo. *D*, "Vesiculators," such as EHD1 (33, 34), GRAF1 (24) and the lipid modifier cPLA2α (33), constrict the TRE by mechanical force and changes in lipid composition, respectively. *E*, scission gives rise to mobile and small recycling endosomes, which are transported along microtubules toward the PM. It is not clear if any of the membrane "sculpting" proteins remain on the highly-curved recycling endosomes.

Although future studies will be required to dissect the function of DGKα in regulating MHC I trafficking post-internalization and prior to recycling, our study highlights a novel role for this enzyme in the generation of TRE and the subsequent regulation of endocytic recycling.

REFERENCES

1. Antón, L. C., and Yewdell, J. W. (2014) Translating DRiPs: MHC class I immunosurveillance of pathogens and tumors. *J. Leukoc. Biol.* **95,** 551–562
2. Donaldson, J. G., Porat-Shliom, N., and Cohen, L. A. (2009) Clathrin-independent endocytosis: a unique platform for cell signaling and PM remodeling. *Cell. Signal.* **21,** 1–6
3. Mettlen, M., Stoeber, M., Loerke, D., Antonescu, C. N., Danuser, G., and Schmid, S. L. (2009) Endocytic accessory proteins are functionally distinguished by their differential effects on the maturation of clathrin-coated pits. *Mol. Biol. Cell* **20,** 3251–3260
4. Tebar, F., Sorkina, T., Sorkin, A., Ericsson, M., and Kirchhausen, T. (1996) Eps15 is a component of clathrin-coated pits and vesicles and is located at the rim of coated pits. *J. Biol. Chem.* **271,** 28727–28730
5. Adams, A., Thorn, J. M., Yamabhai, M., Kay, B. K., and O'Bryan, J. P. (2000) Intersectin, an adaptor protein involved in clathrin-mediated endocytosis, activates mitogenic signaling pathways. *J. Biol. Chem.* **275,** 27414–27420
6. Yamabhai, M., Hoffman, N. G., Hardison, N. L., McPherson, P. S., Castagnoli, L., Cesareni, G., and Kay, B. K. (1998) Intersectin, a novel adaptor protein with two Eps15 homology and five Src homology 3 domains. *J. Biol. Chem.* **273,** 31401–31407
7. Gad, H., Ringstad, N., Löw, P., Kjaerulff, O., Gustafsson, J., Wenk, M., Di Paolo, G., Nemoto, Y., Crun, J., Ellisman, M. H., De Camilli, P., Shupliakov,

O., and Brodin, L. (2000) Fission and uncoating of synaptic clathrin-coated vesicles are perturbed by disruption of interactions with the SH3 domain of endophilin. *Neuron* **27,** 301–312
8. Hinshaw, J. E., and Schmid, S. L. (1995) Dynamin self-assembles into rings suggesting a mechanism for coated vesicle budding. *Nature* **374,** 190–192
9. Pelkmans, L., Fava, E., Grabner, H., Hannus, M., Habermann, B., Krausz, E., and Zerial, M. (2005) Genome-wide analysis of human kinases in clathrin- and caveolae/raft-mediated endocytosis. *Nature* **436,** 78–86
10. Kawasaki, T., Kobayashi, T., Ueyama, T., Shirai, Y., and Saito, N. (2008) Regulation of clathrin-dependent endocytosis by diacylglycerol kinase delta: importance of kinase activity and binding to AP2alpha. *Biochem. J.* **409,** 471–479
11. Mérida, I., Avila-Flores, A., and Merino, E. (2008) Diacylglycerol kinases: at the hub of cell signalling. *Biochem. J.* **409,** 1–18
12. Antonescu, C. N., Danuser, G., and Schmid, S. L. (2010) Phosphatidic acid plays a regulatory role in clathrin-mediated endocytosis. *Mol. Biol. Cell* **21,** 2944–2952
13. Giridharan, S. S., Cai, B., Vitale, N., Naslavsky, N., and Caplan, S. (2013) Cooperation of MICAL-L1, syndapin2, and phosphatidic acid in tubular recycling endosome biogenesis. *Mol. Biol. Cell* **24,** 1776–1790
14. Rainero, E., Caswell, P. T., Muller, P. A., Grindlay, J., McCaffrey, M. W., Zhang, Q., Wakelam, M. J., Vousden, K. H., Graziani, A., and Norman, J. C. (2012) Diacylglycerol kinase α controls RCP-dependent integrin trafficking to promote invasive migration. *J. Cell Biol.* **196,** 277–295
15. Brown, F. D., Rozelle, A. L., Yin, H. L., Balla, T., and Donaldson, J. G. (2001) Phosphatidylinositol 4,5-bisphosphate and Arf6-regulated membrane traffic. *J. Cell Biol.* **154,** 1007–1017
16. Jović, M., Naslavsky, N., Rapaport, D., Horowitz, M., and Caplan, S. (2007) EHD1 regulates beta1 integrin endosomal transport: effects on focal adhesions, cell spreading and migration. *J. Cell Sci.* **120,** 802–814
17. Naslavsky, N., Weigert, R., and Donaldson, J. G. (2003) Convergence of non-clathrin- and clathrin-derived endosomes involves Arf6 inactivation and changes in phosphoinositides. *Mol. Biol. Cell* **14,** 417–431
18. Jovanovic, O. A., Brown, F. D., and Donaldson, J. G. (2006) An effector domain mutant of Arf6 implicates phospholipase D in endosomal membrane recycling. *Mol. Biol. Cell* **17,** 327–335
19. Caplan, S., Naslavsky, N., Hartnell, L. M., Lodge, R., Polishchuk, R. S., Donaldson, J. G., and Bonifacino, J. S. (2002) A tubular EHD1-containing compartment involved in the recycling of major histocompatibility complex class I molecules to the plasma membrane. *EMBO J.* **21,** 2557–2567
20. Sharma, M., Naslavsky, N., and Caplan, S. (2008) A role for EHD4 in the regulation of early endosomal transport. *Traffic* **9,** 995–1018
21. Söderberg, O., Gullberg, M., Jarvius, M., Ridderstråle, K., Leuchowius, K. J., Jarvius, J., Wester, K., Hydbring, P., Bahram, F., Larsson, L. G., and Landegren, U. (2006) Direct observation of individual endogenous protein complexes in situ by proximity ligation. *Nat Methods* **3,** 995–1000
22. Naslavsky, N., Weigert, R., and Donaldson, J. G. (2004) Characterization of a nonclathrin endocytic pathway: membrane cargo and lipid requirements. *Mol. Biol. Cell* **15,** 3542–3552
23. Donaldson, J. G., and Williams, D. B. (2009) Intracellular assembly and trafficking of MHC class I molecules. *Traffic* **10,** 1745–1752
24. Cai, B., Xie, S., Caplan, S., and Naslavsky, N. (2014) GRAF1 forms a complex with MICAL-L1 and EHD1 to cooperate in tubular recycling endosome vesiculation. *Front. Cell Dev. Biol.* **2,** 1–14
25. Ezratty, E. J., Bertaux, C., Marcantonio, E. E., and Gundersen, G. G. (2009) Clathrin mediates integrin endocytosis for focal adhesion disassembly in migrating cells. *J. Cell Biol.* **187,** 733–747
26. Ylänne, J., Huuskonen, J., O'Toole, T. E., Ginsberg, M. H., Virtanen, I., and Gahmberg, C. G. (1995) Mutation of the cytoplasmic domain of the integrin beta 3 subunit. Differential effects on cell spreading, recruitment to adhesion plaques, endocytosis, and phagocytosis. *J. Biol. Chem.* **270,** 9550–9557
27. Sharma, M., Giridharan, S. S., Rahajeng, J., Naslavsky, N., and Caplan, S. (2009) MICAL-L1 links EHD1 to tubular recycling endosomes and regulates receptor recycling. *Mol. Biol. Cell* **20,** 5181–5194
28. Shindou, H., Hishikawa, D., Harayama, T., Yuki, K., and Shimizu, T. (2009) Recent progress on acyl CoA: lysophospholipid acyltransferase research. *J. Lipid Res.* **50,** S46–S51
29. Donaldson, J. G. (2009) Phospholipase D in endocytosis and endosomal recycling pathways. *Biochim Biophys Acta* **1791,** 845–849
30. Naslavsky, N., Boehm, M., Backlund, P. S., Jr., and Caplan, S. (2004) Rabenosyn-5 and EHD1 interact and sequentially regulate protein recycling to the plasma membrane. *Mol. Biol. Cell* **15,** 2410–2422
31. Naslavsky, N., Rahajeng, J., Sharma, M., Jovic, M., and Caplan, S. (2006) Interactions between EHD proteins and Rab11-FIP2: a role for EHD3 in early endosomal transport. *Mol. Biol. Cell* **17,** 163–177
32. Rahajeng, J., Giridharan, S. S., Cai, B., Naslavsky, N., and Caplan, S. (2012) MICAL-L1 is a tubular endosomal membrane hub that connects Rab35 and Arf6 with Rab8a. *Traffic* **13,** 82–93
33. Cai, B., Caplan, S., and Naslavsky, N. (2012) cPLA2alpha and EHD1 interact and regulate the vesiculation of cholesterol-rich GPI-anchored protein-containing endosomes. *Mol. Biol. Cell* **23,** 1874–1888
34. Cai, B., Giridharan, S. S., Zhang, J., Saxena, S., Bahl, K., Schmidt, J. A., Sorgen, P. L., Guo, W., Naslavsky, N., and Caplan, S. (2013) Differential roles of C-terminal Eps15 homology domain proteins as vesiculators and tubulators of recycling endosomes. *J. Biol. Chem.* **288,** 30172–30180